Spin polarons in the t-J model

Gerardo Martínez and Peter Horsch
Max-Planck-Institut für Festkörperforschung, Heisenbergstrasse 1, D-7000 Stuttgart 80, Federal Republic of Germany
(Received 7 November 1990)

The motion of a single hole in a two-dimensional Heisenberg antiferromagnet (AF) is studied in a representation where holes are described as spinless fermions (holons) and spins as normal bosons. Assuming long-range AF order the spin dynamics is treated in linear spin-wave theory. The formulation highlights the close relation with the conventional polaron problem. The holon Green's function is calculated self-consistently within the Born approximation using finite-cluster geometries for the numerical solution. As a remarkable result we find close agreement with the spectral function $A(k,\omega)$ of a hole calculated by exact diagonalization methods. $A(k,\omega)$ is characterized by a narrow quasiparticle (QP) peak at the low-energy side of the spectrum, which is well separated from the incoherent part for large enough J values. A complete characterization of our solution is given, including the spectral weight, the dispersion relation, and effective masses of the QP state. A finite-size-scaling study gives a nonvanishing spectral weight of the QP in the thermodynamic limit for values J/t typical for copper oxide superconductors. Our calculations indicate that the self-consistent Born approximation is a valuable scheme for characterizing the dynamics of a hole in the t-J model, even in the strong-coupling regime.

I. INTRODUCTION

An accurate description of the properties of charge carriers in hole-[1] and electron-doped[2] high-temperature superconductors (HTSC's) arising from their interaction with the spin of the Cu atoms ($S=\frac{1}{2}$) seems to be crucial for the understanding of superconductivity in these materials. The undoped reference materials such as La_2CuO_4 are antiferromagnetic (AF) insulators and are well described by the isotropic spin-$\frac{1}{2}$ Heisenberg model.[3] This is a direct consequence of strong correlations on the Cu sites leading to a Cu configuration close to d^9. The strong interaction between carriers and spins is evident from the disappearance of antiferromagnetic long-range order at very low doping concentration.[3] It has been suggested early on by Anderson[4] that the single-band Hubbard model, i.e., including only the Cu sites of the CuO_2 planes, may serve as the generic model describing the essential physics of the charge carriers in HTSC's. The t-J model considered here follows in the large-U limit by projecting out doubly occupied configurations:[5]

$$H_{t\text{-}J}=-t\sum_{\langle i,j\rangle,\sigma}\left(\tilde{c}^{\dagger}_{i,\sigma}\tilde{c}_{j,\sigma}+\text{H.c.}\right)+J\sum_{\langle i,j\rangle}\left[\left(S^z_iS^z_j-\frac{n_in_j}{4}\right)+\frac{\alpha}{2}\left(S^+_iS^-_j+S^-_iS^+_j\right)\right]. \tag{1}$$

The model is characterized by an antiferromagnetic superexchange J and a kinetic energy with the constraint of no double occupancy, i.e., $\tilde{c}_{i,\sigma}=c_{i,\sigma}(1-n_{i,-\sigma})$. For later convenience we allow here for the anisotropic case, i.e., the Heisenberg (Ising) limit is given by $\alpha=1(0)$, respectively. We call it the t-J^z model when in the Ising limit. The connection of the single-band model to the more realistic Emery model[6] has been clarified by Zhang and Rice[7] and others.[8,9]

The existence of quasiparticles (QP's) has been shown in a number of numerical diagonalization studies of the single-particle spectral function for two dimensions.[9–13] These spectra are characterized by a QP peak at low energy well separated from the broad, incoherent part of the spectrum which has a width of about 6–7t. The coherent propagation of the QP is described by a dispersion relation E_k resulting from effective nearest- and next-nearest-neighbor hopping processes on the same sublattice.[9] The minimum energy of E_k is at $\mathbf{k}=(\pm\pi/2,\pm\pi/2)$.

Whereas considerable insight in the properties of these strongly correlated systems has been achieved by the above-mentioned diagonalization — and also by Monte Carlo calculations, no comparable progress has been made by analytical methods. In particular, the existing analytical approaches and also the more recent concepts, e.g., auxiliary boson methods, have not yet been checked critically against the wealth of spectral data obtained by the numerical methods.

We follow here an approach proposed by Schmitt-Rink, Varma, and Ruckenstein[14] which is based on the approximate diagonalization of the Heisenberg part of Eq. (1) via Holstein-Primakoff transformation. The kinetic part in Eq. (1) rewritten in terms of spinless hole (holons) and spin-wave operators yields the coupling between holes and spin waves. The form of the Hamiltonian is thus similar to that of the polaron problem. A detailed investigation of the single-particle Green's function based on a "dominant pole approximation" has been given recently by Kane, Lee, and Read.[15] An alternative formulation

has been suggested by Su *et al.*[16] using a Bogoliubov–de Gennes type of formalism. More recently, a similar approach has been applied to the spin-fermion Hamiltonian for the CuO_2 planes,[17] while the related ferromagnetic problem was studied in detail in the context of the *s-d* Hamiltonian.[18]

The purpose of our work is to demonstrate that in fact the most elementary self-consistent Born approximation of this problem yields spectral functions for the two-dimensional (2D) case in good quantitative agreement with previous numerical diagonalization studies for small systems. Hence this approach may provide a valuable scheme for further work on spectral properties, quasiparticle interactions, etc. A preliminary report has been given elsewhere.[19]

We may therefore understand the appearance of a bound state, i.e., the QP, as a consequence of the holon-spin-wave coupling similar to the standard polaron problem. An interesting aspect of this formulation of the t-J model is the absence of a free kinetic energy for the spinless fermions. The coherent propagation of the QP, with a bandwidth $W \simeq J$ for $J < t$, is a result of the coupling to spin waves. This is different from the usual notion in the polaron problem, where the free (band) mass becomes renormalized due to the coupling of phonons. Here instead it is the coupling to the spin waves which is the only source for the dispersion of the QP. This does not invalidate the explanation of the QP in terms of the "string picture,"[20] where the hole is surrounded (with a certain amplitude) by strings of flipped spins. The spin-correlation function around the spin polaron remains antiferromagnetic, contrary to the quite popular concept of a ferromagnetic polaron,[21,22] where the hole is assumed to move in a ferromagnetic region.

The paper is organized as follows: Section II gives an outline of the reformulation of the Hamiltonian in terms of spinless fermions and spin waves. Section III contains a description of the self-consistent Born approximation, the analysis of higher-order vertex corrections, and the explicit discussion of certain limiting cases. Numerical results for self-energies and spectral functions are given in Sec. IV. This section also summarizes the results for the QP state and related quantities, including the spectral weight, QP dispersion, effective masses, bandwidth and total energies for the perturbative and nonperturbative regime, that is, large and small J/t. Section V discusses the relation of our results to angular resolved photoemission and further experiments. We summarize our results in Sec. VI. An appendix gives some details of the calculation of the holon Green's function.

II. t-J MODEL IN TERMS OF SPINLESS FERMIONS AND SPIN-WAVE OPERATORS

Our aim is the calculation of the single-particle Green's function

$$G_\sigma(k,\omega) = \left\langle \psi_0 \left| c^\dagger_{k\sigma} \frac{1}{\omega - H + E_0} c_{k\sigma} \right| \psi_0 \right\rangle \tag{2}$$

for a hole propagating in a fluctuating spin background as described by the Heisenberg AF (HAF) defined in Eq. (1). To arrive at this goal, it will be profitable first to diagonalize the spin Hamiltonian H_J, at least approximately.

Following this physically motivated strategy we properly include the dynamics, i.e., the spin-wave excitations, and moreover the effect of the zero-point motions in $|\psi_0\rangle$ will be automatically included in the calculation of $G_\sigma(k,\omega)$.

The transformation to spin waves is performed within linear-spin-wave (LSW) theory,[23,24] although this approach may appear questionable in 2D and for $S = \frac{1}{2}$. However, a series of recent numerical studies have shown[25,26] that even for this subtle case, i.e., 2D and $S = \frac{1}{2}$, the predictions of LSW theory are qualitatively correct and quantities such as the sublattice magnetization $\langle S^z_i \rangle$ and the spin-wave velocity[25] are only slightly renormalized.

To simplify the notation it is convenient to perform first a rotation of the spins on the B sublattice by 180° about the S^x axis:[27]

$$S^\pm_j \to S^\mp_j, \quad S^z_j \to -S^z_j, \quad c_{j\sigma} \to c_{j-\sigma}, \quad j \in B. \tag{3}$$

This canonical transformation changes the Néel configuration $|\uparrow\downarrow\uparrow\downarrow\cdots\rangle$ into a ferromagnetic state with all spins up and removes the further necessity to distinguish between sublattices. The Hamiltonian then has the form $H = H_t + H_J$, with

$$H_t = -t \sum_{\langle i,j\rangle,\sigma} (1 - n_{i-\sigma})\, c^\dagger_{i\sigma} c_{j-\sigma} (1 - n_{j\sigma}) + \text{H.c.}, \tag{4}$$

$$H_J = J \sum_{\langle i,j\rangle} \left(\frac{\alpha}{2} \left(S^+_i S^+_j + S^-_i S^-_j \right) - S^z_i S^z_j - \frac{n_i n_j}{4} \right). \tag{5}$$

Next we introduce Bose operators a_i by means of Holstein-Primakoff transformation, i.e., for $S = \frac{1}{2}$:

$$\begin{aligned} S^+_i &= \sqrt{(1 - a^\dagger_i a_i)}\; a_i \sim a_i, \\ S^-_i &= a^\dagger_i \sqrt{(1 - a^\dagger_i a_i)} \sim a^\dagger_i \\ S^z_i &= \tfrac{1}{2} - a^\dagger_i a_i. \end{aligned} \tag{6}$$

The linear approximation provides a rather good description of the spin-dynamics as mentioned previously. Also a mean-field consideration leads to a similar expectation, as $\sqrt{1 - \langle a^\dagger_i a_i \rangle}$ is close to one, although the spin deviations are not small in 2D, i.e., $\langle a^\dagger_i a_i \rangle = \frac{1}{2} - \langle S^z_i \rangle \simeq 0.2$.

Following Ref. 14 we define creation operators for spinless holes

$$h^\dagger_i = c_{i\uparrow} \tag{7}$$

and express the fermion operator $c_{i\downarrow}$ as a composite operator

$$c_{i\downarrow} = h^\dagger_i S^+_i. \tag{8}$$

The *local*-fermion Hilbert space (excluding double occu-

pancy $|\uparrow\downarrow\rangle$) is thereby mapped onto the product space $|\text{hole}\rangle \otimes |\text{spin}\rangle$, with $n_h = 0, 1$ and $s = \pm\frac{1}{2}$.

In spin-holon notation there is a spin at each site even in the presence of a hole, and spin and holon operators commute, e.g.,

$$[h_i, S_i^+] = 0. \tag{9}$$

As compared to the original local-fermion Hilbert space, which consists of three states, i.e., $|\uparrow\rangle_F$, $|\downarrow\rangle_F$, and $|0\rangle_F$, there are now four states, namely $|0,\uparrow\rangle$, $|0,\downarrow\rangle$, $|1,\uparrow\rangle$, and $|1,\downarrow\rangle$. Here "1" denotes the presence of a hole.

To guarantee the correct dimensions of the local Hilbert space we may add the *constraint* [C1]: *At a given site there cannot be both a hole and a spin deviation, thereby eliminating* $|1,\downarrow\rangle$. Formally the constraint [C1] may be incorporated by adding

$$H_c = \lambda \sum_i h_i^\dagger h_i a_i^\dagger a_i$$

to the Hamiltonian. For $\lambda \gg 1$ this term removes the unphysical states from the low-energy sector. We shall describe thereafter how this constraint may be included in a diagrammatic expansion.

On the other hand, we would like to stress here that our results for the motion of a hole in a *quantum* AF show that the complete neglect of the constraint [C1] is not a severe approximation. Its proper inclusion in the Ising limit is important, however.

The basic *constraint* [C2] of the t-J model, namely, that no double occupied configurations $|\uparrow\downarrow\rangle$ are created, *viz.*

$$\tilde{c}_{i\uparrow}^\dagger |\downarrow\rangle_F = (1 - n_{i\downarrow})\, c_{i\uparrow}^\dagger |\downarrow\rangle_F = 0, \tag{10}$$

is automatically fulfilled as

$$h_i |0,\downarrow\rangle = 0,$$

and similarly for reversed spin orientations.

Following these steps the Hamiltonian becomes

$$\begin{aligned} H_{tJ} = & -t \sum_{i,j(i)} (h_i h_j^\dagger a_j + \text{H.c.}) \\ & + \frac{J}{4} \sum_{i,j(i)} h_i h_i^\dagger [\alpha(a_i a_j + a_i^\dagger a_j^\dagger) + a_i^\dagger a_i + a_j^\dagger a_j] h_j h_j^\dagger \\ & - \frac{z}{2} JN(s^2 + \tfrac{1}{4})(1-\delta)^2. \end{aligned} \tag{11}$$

Here $j(i)$ denotes the neighboring sites of i and z is the coordination number. The additional factors $h_i h_i^\dagger$ and $h_j h_j^\dagger$ take care of the loss of magnetic energy in the presence of holes. In mean-field approximation we may replace $h_i h_i^\dagger = (1 - h_i^\dagger h_i)$ by $(1-\delta)$, where δ is the concentration of holes.

In Fourier space and after Bogoliubov transformation $\alpha_q = u_q a_q - v_q a_{-q}^\dagger$, we arrive at

$$H_t = \frac{zt}{\sqrt{N}} \sum_{k,q} h_k^\dagger h_{k-q} \alpha_q \left(u_q \gamma_{k-q} + v_q \gamma_k\right) + \text{H.c.}, \tag{12}$$

and

$$H_J = \sum_q \omega_q \alpha_q^\dagger \alpha_q + E_J^0. \tag{13}$$

The spin-wave energy $\omega_q = szJ(1-\delta)^2 \nu_q$ and the Bogoliubov coherence factors are given by the usual expressions in linear spin-wave theory:

$$\nu_q = \sqrt{1 - (\alpha\gamma_q)^2}, \tag{14}$$

$$u_q = \left(\frac{1+\nu_q}{2\nu_q}\right)^{1/2}, \qquad v_q = -\text{sgn}(\gamma_q) \left(\frac{1-\nu_q}{2\nu_q}\right)^{1/2}. \tag{15}$$

Here the function $\gamma_q = \frac{1}{2}(\cos q_x + \cos q_y)$, defining the lattice constant $a = 1$. The ground-state energy E_J^0 in Eq. (13) for $s = \frac{1}{2}$ is given by

$$E_J^0 = -\frac{z}{2} JN(1-\delta)^2 \left[s^2 + \alpha s \left(1 - \frac{1}{N}\sum_q \nu_q\right) + \frac{1}{4}\right]. \tag{16}$$

The similarity of the Hamiltonian with that of the classical polaron problem[28,29] is obvious. Here the spin waves play the role of the phonons. As a noticeable difference we see that a bare term, $H_0 = \sum_k \varepsilon_k h_k^\dagger h_k$, for the spinless fermions is absent. The kinetic term of the t-J model transforms into the coupling term which is proportional to t. Further, the coupling function $M(k,q) = (u_q \gamma_{k-q} + v_q \gamma_k)$ in Eq. (12) vanishes at $\mathbf{q} = 0$ and (π,π), and becomes large at intermediate values of the momentum transfer $\mathbf{q}$. Hence, it is the coupling to the short-wavelength spin fluctuations which is important. As for the copper-oxides $t > J$, the Hamiltonian defined by Eqs. (12) and (13) then poses a strong-coupling problem.

III. SELF-CONSISTENT GREEN'S-FUNCTION APPROACH AND VERTEX CORRECTIONS

A. Born approximation

Given the Hamiltonian of the t-J model in its form of Eqs. (12) and (13), describing holons (spinless fermions) strongly coupled to spin-wave excitations, we will calculate next the holon Green's function:

$$G^h(k,\omega) = \left\langle 0 \left| h_k \frac{1}{\omega - H + E_0} h_k^\dagger \right| 0 \right\rangle. \tag{17}$$

Here the vacuum state for the spinless fermion operators is the state without holes and with respect to the spin-wave operators α_q it is the quantum Néel state

$$|0\rangle_{\text{spin}} = \exp\left(\sum_q \frac{v_q}{u_q} a_q^\dagger a_{-q}^\dagger\right) |N\rangle, \tag{18}$$

where $|N\rangle$ is the classical Néel state, i.e., when we account for the rotation (3) the ferromagnetic state. The electron Green's function in Eq. (2) after substituting

the electron operator $c_{k\sigma}$ according to Eq. (7), appears at first glance as a higher-order Green's function. However, when treating the Bose operators in the mean-field approximation as is shown in the Appendix, G_σ turns out to be equivalent to G^h. That this close correspondence of these two Green's functions persists beyond the mean-field level can be concluded from the remarkable agreement of our results obtained for G^h and the exact diagonalization results for G_σ.[11]

The holon Green's function $G^h(k,\omega) = [\omega - \Sigma(k,\omega)]^{-1}$ can be calculated in a straightforward way within the self-consistent Born approximation,[14,15] which is equivalent to the series of diagrams displayed in Fig. 1. Using standard techniques[28] one finds for the self-energy at zero temperature

$$\Sigma(k,\omega) = \frac{z^2t^2}{N}\sum_q \frac{M^2(k,q)}{\omega - \omega_q - \Sigma(k-q,\omega-\omega_q)}, \qquad (19)$$

where $M^2(k,q) = (u_q\gamma_{k-q} + v_q\gamma_k)^2$. As we are particularly interested in the strong-coupling case ($t > J$) the self-consistent solution of this equation is crucial, and must be performed numerically. From this the spectral function is defined by $A(k,\omega) = -(1/\pi)\mathrm{Im}G^h(k,\omega + i\delta)$ with $\delta \to 0^+$. In practice, we take small values of δ to facilitate the numerical analysis.

We mention the appearance of the analogous equation in the polaron literature,[29] yet we are not aware of a complete solution for the strong-coupling limit.

B. Corrections beyond Born-approximation

The leading vertex corrections are displayed in Fig. 2. We consider here diagrams in real-space representation, as they allow for a direct interpretation in terms of elementary processes. Also we limit ourselves here to the Ising limit ($\alpha = 0$), where we are in the position to compare with analytical results obtained within the retraceable-path approximation (rpa).[21]

First we will review the previous results for Σ obtained within the Born approximation. In the Ising case the equation for the self-energy, Eq. (19), becomes momentum independent as the coupling function M has then the form $M(k,q) = \gamma_{k-q}$. With $\omega_q \to \omega_0 = 2J^z$ and $(1/N)\sum_p \gamma_p^2 = \frac{1}{z}$ one obtains

$$\Sigma(\omega) = \frac{zt^2}{\omega - \omega_0 - \Sigma(\omega - \omega_0)}, \qquad (20)$$

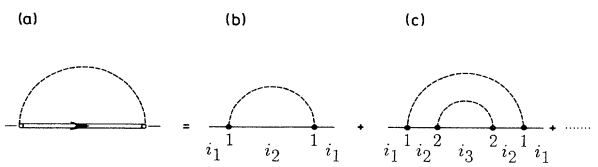

FIG. 1. Leading diagrams included within self-consistent Born approximation. Holon and spin-wave propagators are represented by solid and dashed lines, respectively. The real space coordinate labels pertain to the discussion of the Ising limit in Sec. III B.

which defines a ladder spectrum[30] for $J^z > 0$. See also Fig. 3 below. This may be understood in the string picture,[20] where the hole is bound in a linear potential due to the flipped spins. We mention briefly the results in the Ising case, namely: (i) the number of split peaks scale roughly with $1/J$, (ii) the low-lying ones are separated by $\sim J^{2/3}$, and (iii) most importantly, as a consequence of (i) the spectral weight of the higher peaks decreases with increasing J. For $J^z = 0$ Eq. (20) yields the result $\Sigma(\omega) = \frac{1}{2}(\omega + \sqrt{\omega^2 - 4zt^2})$, thereby a continuous spectrum appears with an incoherent bandwidth of $4t\sqrt{z}$. This result differs from the rpa where a reduced bandwidth $W_{\mathrm{inc}} = 4t\sqrt{z-1}$ is obtained.[21]

It has been noted earlier by Kane, Lee, and Read[15] that the discrepancy in the bandwidth is due to the following difference between the rpa and the Born series in Fig. 1: In rpa a hole at site i_2 arriving from i_1 may hop to any nearest neighbor i_3 except back to $i_3 = i_1$. Until now there is no such restriction in the diagrammatic expansion. If we look more carefully at the diagram, Fig. 1(c), we observe that for $i_3 = i_1$ the hole has created two spin deviations at sites i_1 and i_2, while hopping from i_1 to i_2 and back to i_1. Of course this process is unphysi-

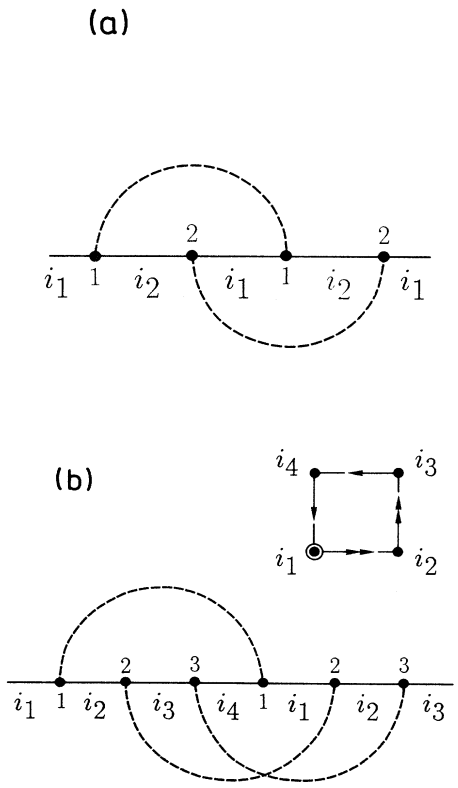

FIG. 2. Vertex corrections omitted in Born approximation. In the Ising case (a) describes an intermediate state with a hole together with a spin deviation at site i_1. Diagram (b) describes the propagation of a hole around a plaquette (clockwise or counterclockwise) from site i_1 to a next-nearest neighbor site i_3. This process leads to the delocalization of the hole in the Ising limit.

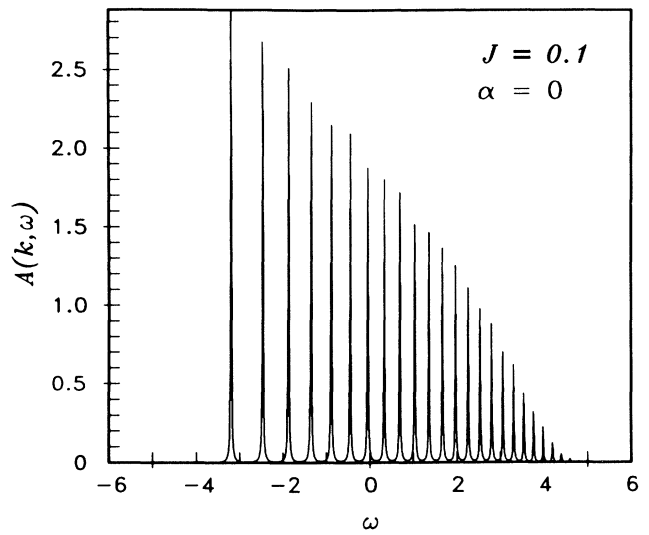

FIG. 3. Spectral function $A(k,\omega)$ for a lattice of 16×16 sites in the t-J^z model and for $J = 0.1t$. To obtain this dispersionless ladder spectrum Eq. (20) was iterated more than 100 times using a broadening $\delta = 0.01t$. Our unit of energy is $t = 1$.

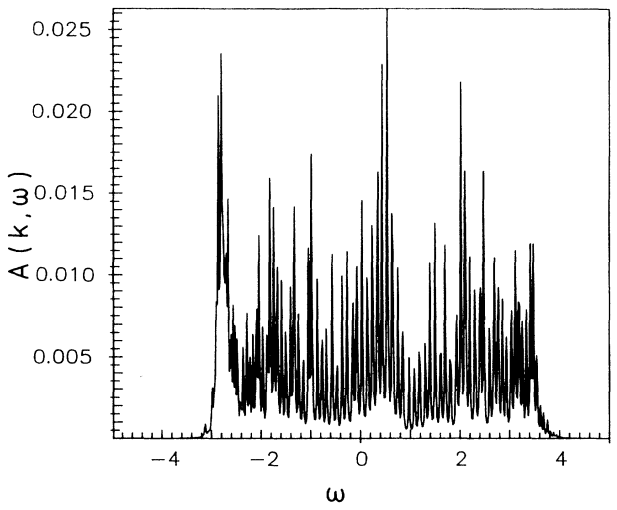

FIG. 4. Exact diagonalization result for the spectral function $A(k,\omega)$ of the t-J^z model in a 4×4 cluster at wave vector $\mathbf{k} = (\pi/2, \pi/2)$ and for a value $J = 0.1t$, using a constant $\delta = 0.01t$.

cal. In the present framework it is the *constraint* [C1] which requires this diagram to be excluded for $i_3 = i_1$. It is straightforward to include the constraint also in all higher-order diagrams of the Born series (Fig. 1). If we do so we then arrive at

$$\Sigma(\omega) = \frac{zt^2}{\omega - \omega_0 - [(z-1)/z]\Sigma(\omega - \omega_0)}, \tag{21}$$

in agreement with the retraceable-path approximation.

Turning now to the self-energy contributions in Fig. 2 which contain vertex corrections, we realize that the first diagram, Fig. 2(a), again violates the constraint [C1]. This diagram contains a hole at i_1 in an intermediate state together with a spin deviation at the same site, hence it should be dropped for $\alpha = 0$.

The next diagram, Fig. 2(b) of order t^6/J_z^5, is interesting as it describes the motion of a hole around an elementary plaquette creating spin deviations at i_1, i_2, and i_3 and annihilating them in the *same* sequence. Thereby, the hole has moved from i_1 to i_3. This process, as discussed by Trugman,[31] leads to the delocalization of the hole in the Ising limit.

In fact due to these processes the complete result for $A(k,\omega)$ in the Ising limit is not a pure ladder spectrum for $J^z < t$. A spectral function obtained by exact diagonalization is shown for comparison in Fig. 4 (see also Ref. 11). Equation (21) is merely the result obtained on a Bethe lattice, that is, excluding processes with closed loops.

The discussion of the Ising case also demonstrates the necessity to solve the equation for the self-energy (19) self-consistently, as the problem must be treated to infinite order in perturbation theory. Only then is the correct analytical structure for $\Sigma(\omega)$ obtained in the strong- and intermediate-coupling regimes.

Although we will not go into a discussion of the isotropic case here, we wish to point out that the contribution from vertex corrections seems not to be that important for $\alpha = 1$. The delocalization of holes is mainly a result of the action of the spin-flip terms in H_J, whereas the Trugman processes give only a minor contribution to the coherent motion for not too large values of J,[11] and are completely irrelevant for $J > t$. The unimportance of the constraint [C1] may be understood as a consequence of the propagation of the spin deviations in this case.

It is also remarkable that the solution of Eq. (19) for the isotropic case and $J \to 0$ already gives a reduced bandwidth $W_{\text{inc}} \simeq 7t$, without taking into account the constraint [C1], as is shown in the next section. In the Ising limit, on the other hand, it is crucial to include this constraint to obtain the reduction of the bandwidth.

IV. NUMERICAL SOLUTION AND RESULTS FOR THE t-J MODEL IN 2D

A. Spectral functions

This section gives a description of the numerical results obtained for the integral equation (19) in two-dimensions. Selecting different cluster sizes the wave numbers $\mathbf{k}$ and $\mathbf{q}$ in Eq. (19) are chosen as for a cluster with N sites and periodic boundary conditions. This choice allows us a detailed comparison with results from exact diagonalization studies for small clusters, which are free of any approximation. A systematic study of the convergence of the results with increasing N is also feasible. We reduce as much as possible the numerical effort by exploiting all possible symmetries. This amounts for instance in a calculation of a 16×16 lattice to deal only with 25 k points in the irreducible wedge of the AF Brillouin zone (BZ). A typical mesh for the energy scale ω consists of 1000 points to achieve sufficient energy resolution. The sum

rules on $A(k,\omega)$ were satisfied to within better than 0.1% at each iteration. The number of iterations required in the small-J limit was typically 50–80 and of course much less for $J > t$.

In Fig. 5 we show spectral functions for a lattice of 4×4 sites and for $J = 0.2$ (we will refer all quantities in units of t from now on). To allow for a direct comparison with exact diagonalization results,[11] where the excitation energies $\omega_{n\mathbf{k}} = E_n^{N\pm1}(\mathbf{k}) - E_0^N$ in a photoemission process refer to the ground state of the N-particle system, we have included in our calculations of Fig. 5 (only for this case) the energy shift resulting from the change of the ground-state energy E_J^0, Eq. (16), when removing a spin. As in the exact diagonalization study, see Fig. 6 for comparison, we observe that a well separated QP peak is obtained at the bottom part of the spectrum with its minimum energy at $(\pi/2,\pi/2)$.

Several features deserve a discussion with this cluster. First, it is well known that an accidental degeneracy makes coincidence of $(\pi/2,\pi/2)$ and $(\pi,0)$ states in this particular geometry, so the minimum QP energy cannot be distinguished from these two points. Secondly, since there is a degeneracy of $(0,0)$ and (π,π) states in our broken symmetry treatment, we thus have only three different k points, the others are shown in the insets of Fig. 5: $(0,0)$ and $(\pi/2,0)$. Consequently, the density of states would then have two main peaks at the bottom part (a third coming from $(0,0)$ has a very small intensity), as compared with Fig. 11 of Ref. 11. Thirdly, as in the exact calculation, the solution found for the spectral function at $(0,0)$ has its main spectral weight at about $\omega \simeq 0$ (see inset in Fig. 5), a feature which is shared by all states close to the Γ point, as will be seen below.

We change now to the study of a bigger cluster. Results for the spectral function in a lattice of 16×16 sites and $J = 0.4$ are shown in Fig. 7. The situation in this case, as compared to Fig. 5, is that the QP peak is separated from a broad continuum, relatively structureless, except for those states close to $(0,0)$. At $(\pi/2,\pi/2)$ there are also some extra small peaks in the depletion between the QP peak and the incoherent part [the energy interval $-2 < \omega < -1$ in Fig. 7(b)], which presumably will change into a continuum with small spectral weight for even larger systems. Spectra at $(\pi/2,\pi/2)$ and $(\pi,0)$ are now different and the minimum QP energy is at $(\pi/2,\pi/2)$ and the maximum at $(0,0)$. The total density of states, Fig. 7(c), reveals the band of coherent states at the low-energy side of the spectrum, with an incoherent background starting at about $\omega \approx -1.5$.

The corresponding data of $\Sigma(k,\omega)$ for a lattice of 16×16 sites and $J = 0.4$ is shown in Fig. 8. Upper panels (a) and (b) show real and imaginary parts of Σ for $\mathbf{k} = (0,0)$ and lower panels (c) and (d) the same for $\mathbf{k} = (\pi/2,\pi/2)$. The solution is qualitatively different

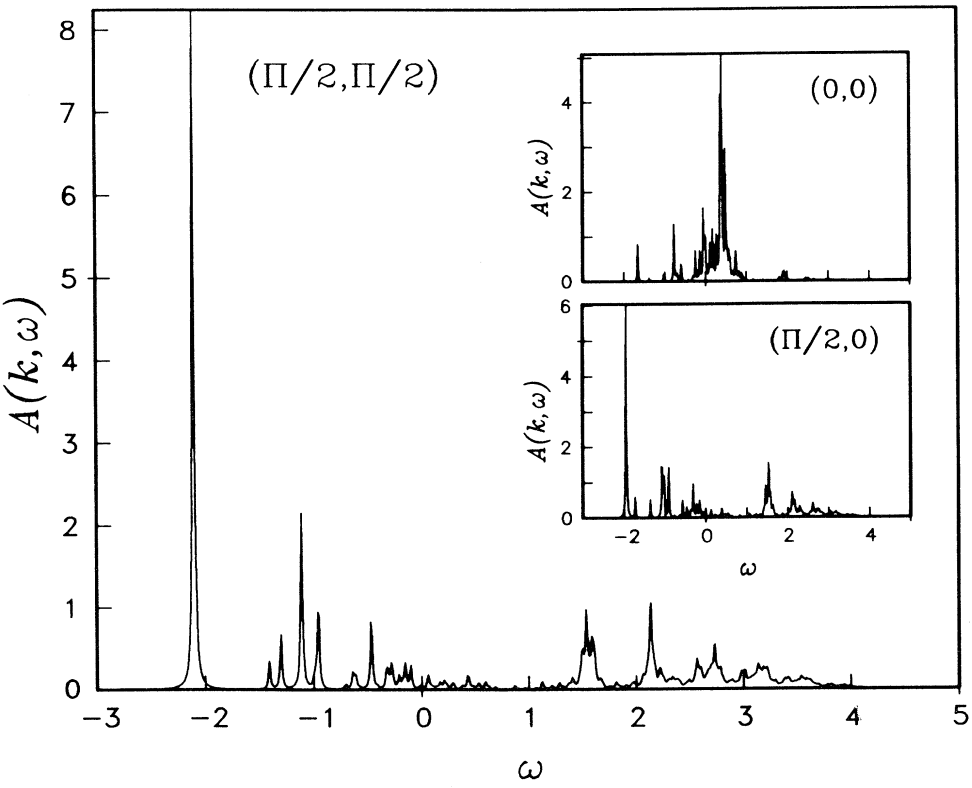

FIG. 5. Spectral function $A(k,\omega)$ at wave vector $\mathbf{k} = (\pi/2,\pi/2)$ for a cluster of 4×4 sites and $J = 0.2$ as calculated in Born approximation. Insets: $\mathbf{k} = (0,0)$ and $\mathbf{k} = (\pi/2,0)$. Our results have been shifted by the constant energy describing the change of the ground state, Eq. (16) ~ 0.28 in this case, to compare with the results from exact diagonalization studies of Fig. 6.

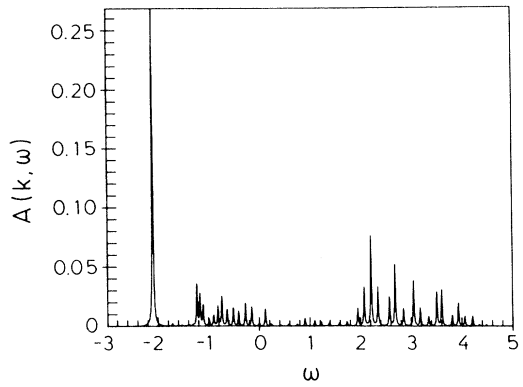

FIG. 6. Exact diagonalization result for the spectral function $A(k,\omega)$ of one hole in the t-J model in the *singlet* sector using a 4×4 cluster at $\mathbf{k} = (\pi/2, \pi/2)$, for $J = 0.2$. Reproduced from Ref. 11.

in these two cases. Many narrow oscillations are seen at $(\pi/2, \pi/2)$ slightly above the QP energy. The main effect of these oscillations is to reduce spectral weight above the QP peak.

We consider now briefly the limit of small J. Results for $J = 0.01$ are given in Fig. 9. The total density of states in Fig. 9(c) has the form of a broad continuum with a reduced width $W_{\rm inc} \leq 7t$, similar to the rpa solution for the propagation in a classical Néel background and $J = 0$.[21] In addition, one observes at the low-energy sector small remnants of a ladder spectrum, which is k dependent, superimposed on the continuum.

The reduced width of the continuum in this limit is particularly remarkable in view of the discussion about the t-J^z model, where it turned out crucial to include the constraint [C1] in the Born approximation.

Again the results close to $\mathbf{k} = (0,0)$ and (π, π) differ from those at other k points. At $\mathbf{k} = (0,0)$, as seen from Fig. 9(a), the spectral function $A(k,\omega)$ is described by a broad Lorentzian-like peak centered at $\omega = 0$, with tails stretching to the band edges. Both features are a consequence of the coherence factors which determine $M(k,q)$ and which reflect the spin dynamics of the HAF. We also note that this differs from results obtained in perturbation theory around the Ising limit taking $\alpha = H_\perp/H_z$ as small parameter.[15] Finally, we observe a large depletion of states around $\omega = 0$ at $\mathbf{k} = (\pi/2, \pi/2)$, in Fig. 9(b), which is less pronounced than the small-J result in the 4×4 cluster. Hence the strong depletion and even the formation of two bands in the exact results for small-J is probably a finite-size effect.

It is interesting to compare the solution for the small J case with that of the Ising limit of Fig. 3. When the spin fluctuations are suppressed ($\alpha = 0$) the incoherent background disappears leading to a discrete ladder spectrum. This is understood in terms of the string picture, where the hole is seen to be bound in a linear potential, as already mentioned. Now, the appearance of the continuum is concomitant with the reduction of the ladder when the spin fluctuations are turned back on. For a given J, the split peaks shrink and reduce their intensity as if an effective $J_{\rm eff} < J$ is acting to produce the ladder at the lowest part of the spectrum. In other words, for small J the spin fluctuations are not fast enough to completely destroy the string which lasts for a time $\sim 1/J$. That is, for $J \ll t$ the hole can perform many hops before the spins can relax.

B. Quantities related to the quasiparticle

We present here some features of the QP peak, such as, e.g., its spectral weight and the dispersion as a function of J, together with a detailed comparison with known results from exact diagonalization for small clusters.

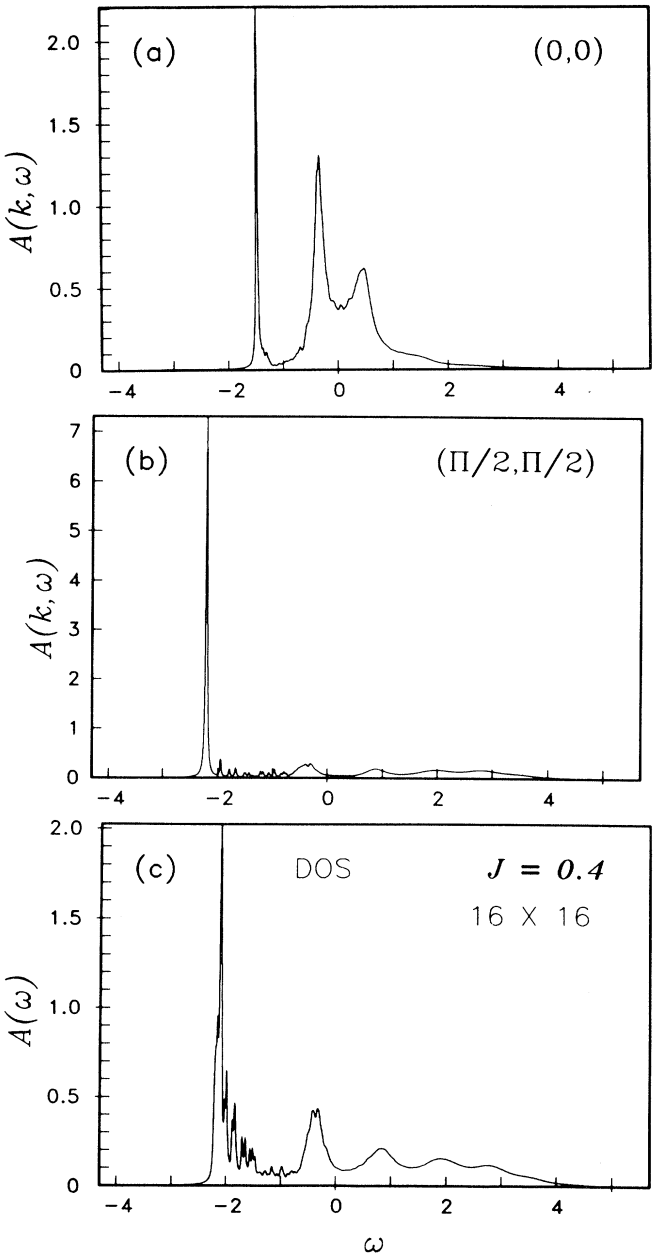

FIG. 7. Spectral functions $A(k,\omega)$ for 16×16 sites and $J = 0.4$: (a) $\mathbf{k} = (0,0)$; (b) $\mathbf{k} = (\pi/2, \pi/2)$, a QP peak at the leftmost part in both spectra is clearly seen separated from a continuum; (c) total density of states $A(\omega) = \sum_k A(k,\omega)$.

The spectral weight of the QP (the integrated area under the QP peak normalized with respect to the total area) is given in Fig. 10 for two values of the wave vectors: at $\mathbf{k} = (0,0)$ and $(\pi/2, \pi/2)$, in the extended region $0 \leq J \leq 8.0$, together with the large-J limit of the expression

$$a(k) = \left. \frac{1}{1 - (\partial/\partial\omega)\Sigma(k,\omega)} \right|_{\omega = E_k}, \tag{22}$$

where the QP energy is given by $E_k = \Sigma(k, E_k)$. Taking Eq. (19) we obtain

$$\frac{\partial}{\partial\omega}\Sigma(k,\omega) = -\frac{z^2t^2}{N}\sum_q M^2(k,q)\left(1 - \frac{\partial\Sigma(k-q,\omega-\omega_q)}{\partial\omega}\right) \Big/ [\omega - \omega_q - \Sigma(k-q,\omega-\omega_q)]^2 .$$

In the perturbative limit $t \ll J$, i.e., when $\omega - \Sigma \ll \omega_q$

$$\frac{\partial\Sigma}{\partial\omega} \approx -\frac{z^2t^2}{N}\sum_q \frac{M^2(k,q)}{\omega_q^2},$$

and hence $a(k)$ is simply given in terms of the coupling function $M(k,q)$ and the magnon dispersion

$$a(k) \cong \frac{1}{1 + (z^2t^2/N)\sum_q M^2(k,q)/\omega_q^2}. \tag{23}$$

This expression approaches 1 for $J \gg t$ and provides a good description of the numerical data also in the intermediate-coupling regime. Even in the strong-

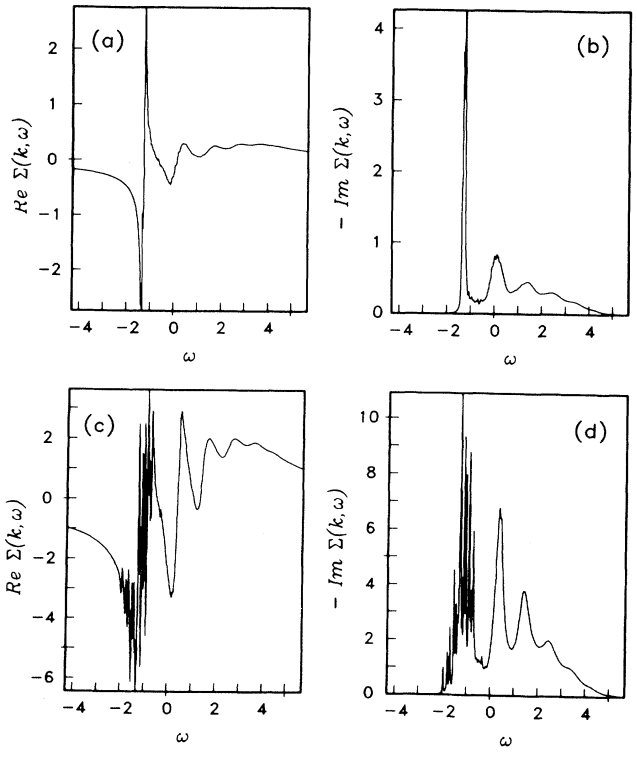

FIG. 8. Real and Imaginary parts of the self-energy $\Sigma(k,\omega)$ for 16×16 sites and $J = 0.4$. Upper panels (a) and (b) corresponding to wave vector $\mathbf{k} = (0,0)$ and lower panels (c) and (d) to $\mathbf{k} = (\pi/2, \pi/2)$.

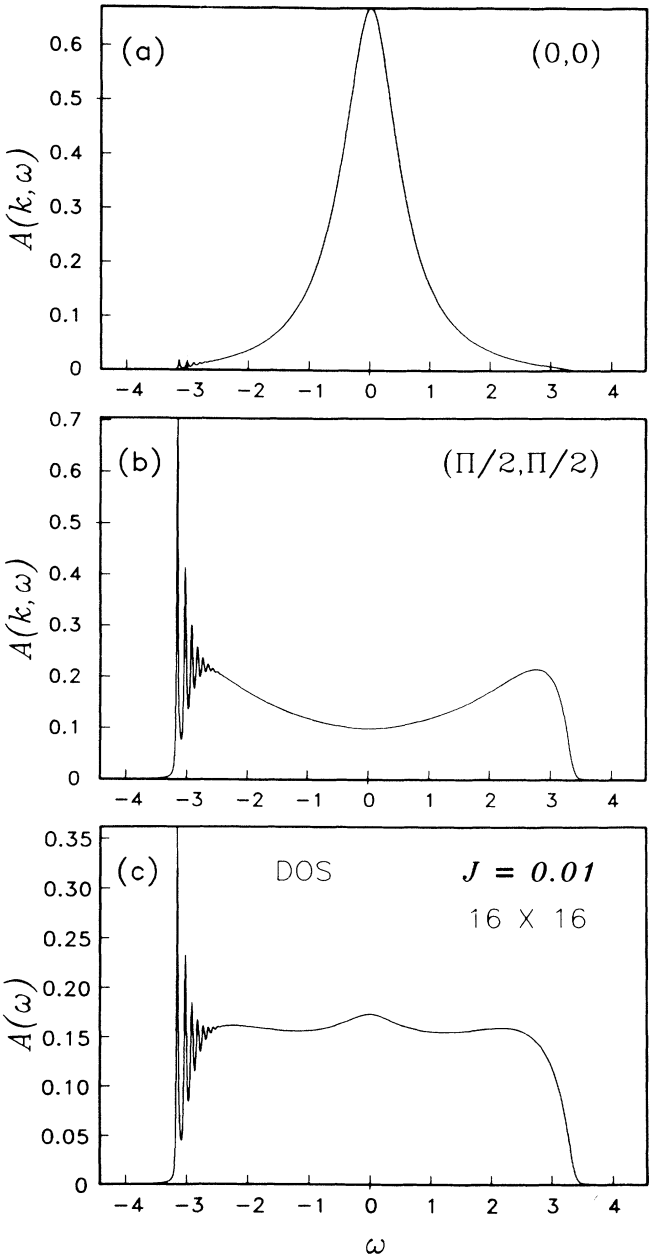

FIG. 9. Spectral functions $A(k,\omega)$ for 16×16 sites and $J = 0.01$: (a) at $\mathbf{k} = (0,0)$, (b) at $\mathbf{k} = (\pi/2, \pi/2)$, and (c) total density of states $A(\omega)$.

coupling limit, where the basic assumption for the derivation of Eq. (23) clearly does not apply, this equation still gives a rough estimate for the spectral weight results in Fig. 10.

The results for $a(k)$ in the strong-coupling regime ($J \leq 1.0$) are shown in Fig. 11 for several k points. These results may be well approximated by a simple power law $a(k) = \lambda J^{\epsilon}$ in this range. Taking their values within $0.01 \leq J \leq 0.5$ we found $a(\pi,0) \simeq 0.71J^{0.70}$ and $a(\pi/2,\pi/2) \simeq 0.63J^{0.667}$. Beyond $J \simeq 1$ a power law cannot be used as the data saturates to 1, and one may use instead Eq. (23). This departure from the fit is indicated with dashed lines in the last portion of the fitting curves of Figs. 10 and 11, respectively. The result for $\mathbf{k} = (0,0)$ is special again as in the diagonalization studies. In this case the spectral weight increases slowly with J as $a(0,0) \simeq 0.89J^{2.25}$ for $0.01 \leq J \leq 0.5$. At $J \sim 1$ the spectral weight for all k values have about the same magnitude. For large J the weight of the QP peak at $\mathbf{k} = (0,0)$ actually becomes the largest (see Table I).

The dispersion relation E_k of QP states, normalized by its bandwidth W along the symmetry lines in the AF BZ, is shown in Fig. 12. The results for $J = 0.01$ and

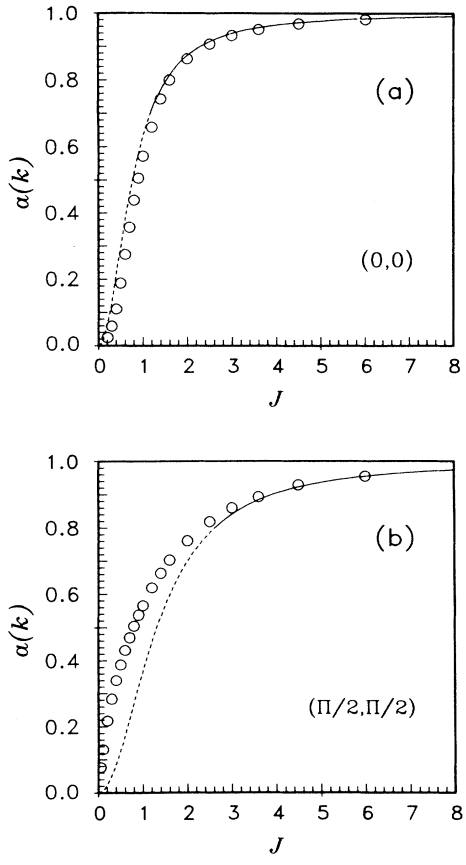

FIG. 10. QP spectral weight $a(k)$ for a 16 × 16 lattice in the parameter range $0.01 \leq J \leq 8.0$: (a) $\mathbf{k} = (0,0)$ and (b) $\mathbf{k} = (\pi/2,\pi/2)$, plotted together with the analytic result for the large-J limit, Eq. (23).

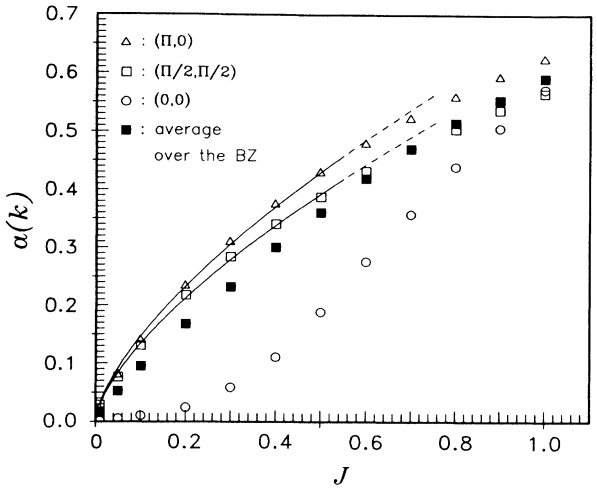

FIG. 11. QP spectral weight $a(k)$ at different k points for a 16 × 16 lattice in the strong-coupling regime $0.01 \leq J \leq 1.0$. The two interpolating curves represent a fit $a(k) = \lambda J^{\epsilon}$ for $\mathbf{k} = (\pi,0)$ and $(\pi/2,\pi/2)$, respectively (see text).

$J = 0.8$ are plotted together with the large-J limit as given by

$$E_k = \Sigma(k, E_k) \simeq -\frac{z^2t^2}{N}\sum_q \frac{M^2(k,q)}{\omega_q}. \tag{24}$$

For all other values of J, the dispersion relation lies within these two boundaries. The main feature of this solution is the local maximum at $(\pi,0)$ and the absolute minimum at $(\pi/2,\pi/2)$. Actually, a saddle point occurs along the symmetry line Γ-M. Hence the dispersion defines hole pockets around $(\pi/2,\pi/2)$. This dispersion relation can be fitted using the following expression

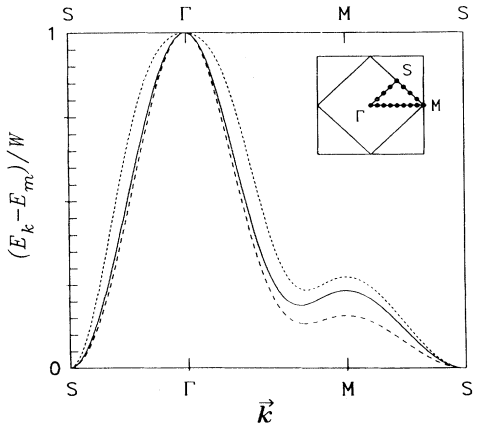

FIG. 12. Dispersion relation E_k of the QP band normalized by the bandwidth $W = E(0,0) - E(\pi/2,\pi/2)$ and $E_m = E(\pi/2,\pi/2)$ along symmetry lines in the AF BZ: large-J limit Eq. (24) (solid line), $J = 0.01$ (short-dashed line), and $J = 0.8$ (long-dashed line). Inset: allowed k points for a 16 × 16 lattice along the symmetry lines in the AF BZ.

TABLE I. Different quantities associated to the quasiparticle measured using a 16×16 lattice as a function of J/t: total energy of QP states E_m at $\mathbf{k} = (\pi/2, \pi/2)$, bandwidth W, relative spectral weights $a(k)$ at different k points and its average over the Brillouin Zone. Energy parameters are in units of t.

J/t	E_m	W	$a(\pi/2,\pi/2)$	$a(\pi,0)$	$a(0,0)$	$\langle a(k)\rangle_{BZ}$
0.01	−3.164	0.027	0.029	0.022	0.001	0.017
0.05	−2.951	0.129	0.076	0.080	0.005	0.052
0.1	−2.785	0.239	0.131	0.140	0.011	0.095
0.2	−2.540	0.430	0.217	0.233	0.024	0.167
0.3	−2.360	0.600	0.284	0.309	0.059	0.232
0.4	−2.209	0.741	0.340	0.374	0.111	0.300
0.5	−2.085	0.850	0.387	0.428	0.188	0.360
0.6	−1.970	0.921	0.431	0.478	0.275	0.418
0.7	−1.867	0.960	0.469	0.521	0.357	0.469
0.8	−1.770	0.981	0.504	0.558	0.439	0.515
0.9	−1.682	0.979	0.538	0.595	0.512	0.558
1.0	−1.600	0.970	0.565	0.624	0.572	0.591
1.2	−1.453	0.940	0.619	0.679	0.658	0.653
1.4	−1.335	0.895	0.663	0.723	0.743	0.703

$$E(k) = x_1 + x_2(\cos k_x + \cos k_y)^2 + x_3(\cos 2k_x + \cos 2k_y), \quad (25)$$

which is motivated by the inclusion of hopping processes to first- and second-nearest neighbors on the same sublattice. The imbalance coefficient, x_3, has been introduced in Eq. (25) to distinguish between a dispersion where the minimum energy for holes is on the Fermi surface for noninteracting electrons ($x_3 = 0$), and a case characterizing hole pockets ($x_3 > 0$).[32] The values found for the parameters x_1, x_2, and x_3 for different J values are given in Table II. Another way of looking at the same quantity is the contour plot in Fig. 13. The "pocketlike" Fermi surface around $(\pm\pi/2, \pm\pi/2)$ is also clearly seen. Here, the hole pockets result from the quantum fluctuations in the ground state and are *not* a consequence of the higher-order processes in t.[31,32] In particular, the pockets are also present for large values of J where the Trugman processes become irrelevant.

From the dispersion of the QP we can calculate effective masses in parallel and perpendicular directions to the magnetic zone boundary at $\mathbf{k} = (\pi/2, \pi/2)$. The results in Table III show a strong anisotropy (of order 4–7) in both directions in the whole range of J values, with the "light" mass $m_\perp = (x_2 + x_3)^{-1}$ and the "heavy" mass $m_\parallel = x_3^{-1}$, written in units of the free band mass $m_0 = (4t)^{-1}$. These results are in agreement with those published earlier.[10] We note that these parameters depend sensitively on the precise form chosen for the fit to the dispersion relation, as the comparison with our previous results (Ref. 19) shows.

The bandwidth W of QP states versus J for different lattice sizes is shown in Fig. 14. We observe only rather small differences between a 4×4 (○) lattice and a 16×16 (●) lattice due to finite-size effects. The results for a 8×8 lattice were not included since they almost coincide with those for 16×16 sites on the scale plotted. The inset gives a comparison with an exact diagonalization study[11] for small values of J. We note that for the exact calculation in a 4×4 cluster W crosses zero at about $J \approx 0.07$. This has been attributed to arise from higher-order processes in t, which contribute in the small-J regime.[11] In the small-J region $0.01 \leq J \leq 0.5$ our numerical results can be interpolated by $W = 1.5J^{0.79}$. The bandwidth W has its maximum value of $0.98t$ at $J = 0.8$, as compared to the variational result, where the maximum is found at $J = 0.73$.[33] The decrease for large values of J can be taken from the perturbative result Eq. (24):

TABLE II. Values of the QP band parameters according to Eq. (25) for a 16×16 lattice as a function of J/t. If the fit includes the hopping processes related to further neighbors they change by less than 2%.

J/t	x_1	x_2	x_3
0.01	−3.160	0.006	0.001
0.05	−2.930	0.026	0.007
0.1	−2.749	0.052	0.012
0.3	−2.305	0.131	0.027
0.5	−2.020	0.180	0.035
0.8	−1.700	0.197	0.043
2.0	−0.998	0.150	0.038
3.6	−0.609	0.094	0.030
10.0	−0.234	0.037	0.013

TABLE III. Effective masses in units of the free band mass $(4t)^{-1}$ at $(\pi/2, \pi/2)$ in parallel and perpendicular directions to the magnetic zone boundary, as a function of J/t.

J/t	$m_\parallel$	$m_\perp$	$m_\parallel/m_\perp$
0.01	1000.0	142.9	7.0
0.05	142.9	30.3	4.7
0.1	83.3	15.6	5.3
0.3	37.0	6.3	5.9
0.5	28.6	4.7	6.1
0.8	23.3	4.2	5.5
2.0	26.3	5.3	5.0
3.6	33.3	8.1	4.1
10.0	76.9	20.0	3.8

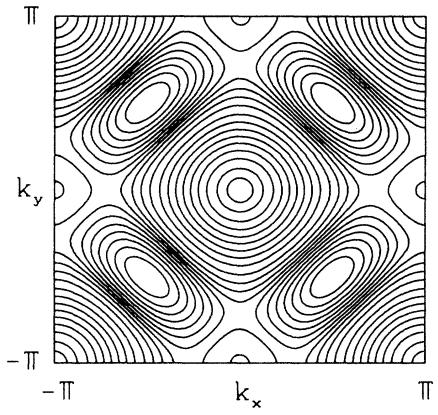

FIG. 13. Contour plot of the dispersion relation of QP states using the large-J limit result, Eq. (24). The minima (hole pockets) are centered at $(\pm\pi/2, \pm\pi/2)$.

$$W = E(0,0) - E(\pi/2,\pi/2) \cong ct^2/J. \tag{26}$$

For the constant we get $c = 2.0$ using the 16×16 lattice. This value is somewhat smaller than the variational result ($c = 2.6$) of Sachdev.[33]

The energy of the minimum of the QP band $E_{\min}(J) = E_m(\pi/2,\pi/2) + \Delta E_J$ as a function of J and for different lattice sizes is given in Fig. 15. The dependence of $E_{\min}(J)$ is again in good agreement with the previous diagonalization results. For example, Dagotto *et al.*[12] found these results well described by the power law $E_{\min}(J) = -3.17 + 2.83J^{0.73}$ in the interval $0.1 < J < 1.0$ for a 4×4 cluster. To compare we have to account for the change ΔE_J of the ground state E_J^0 in the photoemission process. Observing that in Ref. 12 the $n_i n_j/4$ term is absent we obtain for the change of the ground-state energy, Eq. (16), setting $\delta = 1/N$

$$\Delta E_J = Jz\left[s^2 + \alpha s\left(1 - \frac{1}{N}\sum_q \nu_q\right)\right]. \tag{27}$$

Alternatively, one may take $\Delta E_J = zJ|\langle \mathbf{S}_i \cdot \mathbf{S}_{i+1}\rangle|$ from exact diagonalization studies as, e.g., in Ref. 25. The data for $E_{\min}(J)$ is in fact well described by a simple power law over a wide parameter range, i.e., $0.1 \le J \le 1.5$. For the unit cell size 4×4 we find $E_{\min}(J) = -3.11 + 3.05J^{0.69}$. Data for other system sizes are given in Table IV and show that there is good quantitative agreement for this quantity between the self-consistent Born approximation and the exact diagonalization. Further, one may note that the finite-size effects are not very large in this case.

The lifetime of the QP states away from the minimum remains infinite since due to their quadratic dispersion they cannot decay by emission of spin waves. Only if the group velocity of the quasiparticles becomes larger than the spin-wave velocity, $c = d\omega_q/dq = \sqrt{2}J$, the quasiparticles are damped,[15] otherwise conservation of energy and momentum forbids decay processes. It is interesting that for the self-consistent solution, Eq.(25), $|dE_k/dk| < c$ for a large part of the Brillouin zone. Only the states close to Γ and (π,π) appear to be damped as seen in Figs. 7(a)

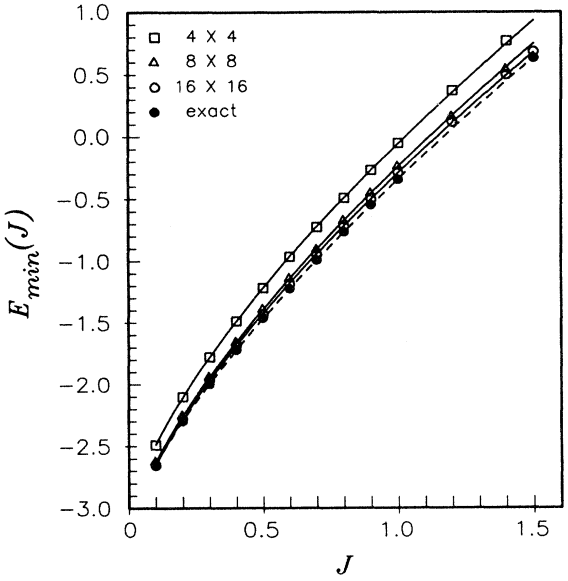

FIG. 15. Total energy of QP states $E_{\min}(J)$ at $(\pi/2,\pi/2)$ vs J for different lattice sizes, together with exact results for 4×4. Our data $E_m(\pi/2,\pi/2)$ have been shifted by ΔE_J for comparison purpose. The curves are a fit to a power law in the region plotted (see text and Table IV).

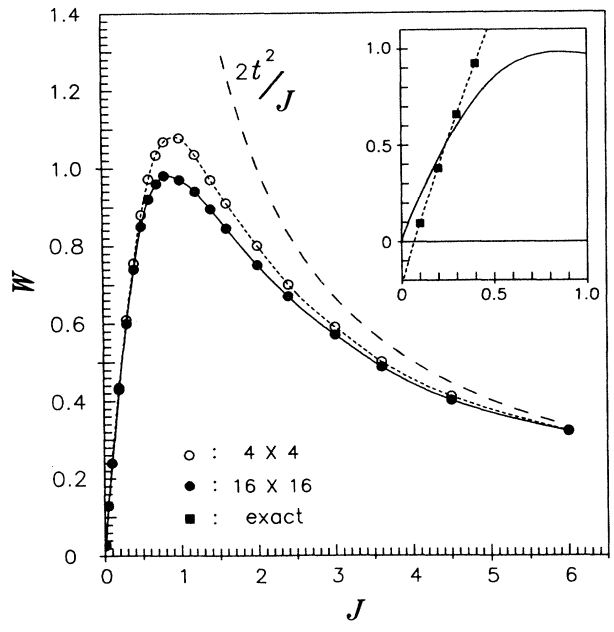

FIG. 14. Bandwidth of QP states W vs J for two lattices 4×4 (o) and 16×16 (•), together with the large-J limit (long-dashed line), Eq. (24). Finite-size effects are small, i.e., data for 8×8 not shown, are already indistinguishable from the results for 16×16. Inset: comparison with exact diagonalization results (Ref. 11) in the range $0.01 \le J \le 1.0$.

TABLE IV. Best constants to describe $E_{\min}(J) = C+\lambda J^{\epsilon}$ for different lattice sizes in the parameter region $0.1 \leq J \leq 1.5$, together with those from exact diagonalization of a 4×4 cluster. Additive constants $\Delta E_J/J$ are also given.

Cluster	C	λ	ϵ	$\Delta E_J/J$[a]
4×4	−3.11	3.05	0.692	1.404
8×8	−3.20	2.96	0.710	1.328
16×16	−3.23	2.94	0.702	1.309
Exact[b]	−3.17	2.83	0.73	

[a]See Ref. 25.
[b]See Refs. 11 and 12.

and 8(b), respectively.

Finally, we have investigated the system size dependence of the spectral weight in the QP peak for $\mathbf{k} = (\pi/2, \pi/2)$, i.e., at the minimum of the dispersion curve. The result is shown in Fig. 16 for the case of $J = 0.4$ (which corresponds to a Hubbard $U = 10$). For 2D a scaling law $a(L) = a_\infty + b/L$, with L the linear dimension, follows by inspection of Eq.(23) for $a(k)$, if we introduce $1/L$ for the lower cutoff of the q integration and furthermore observe that $M^2(\mathbf{k}, \mathbf{q}) \simeq q$ for $q \to 0$. This result is not limited to the perturbative case; a similar scaling law may be found starting from the dominant pole approximation. The numerical data in the range $L = 4$–16, $N = L \times L$, appears to be consistent with such a scaling law. We find a nonzero asymptotic value $a_\infty = 0.317$. Hence, we conclude from this numerical analysis that a single hole in a quantum AF with long-range order propagates as a quasiparticle with finite spectral weight.

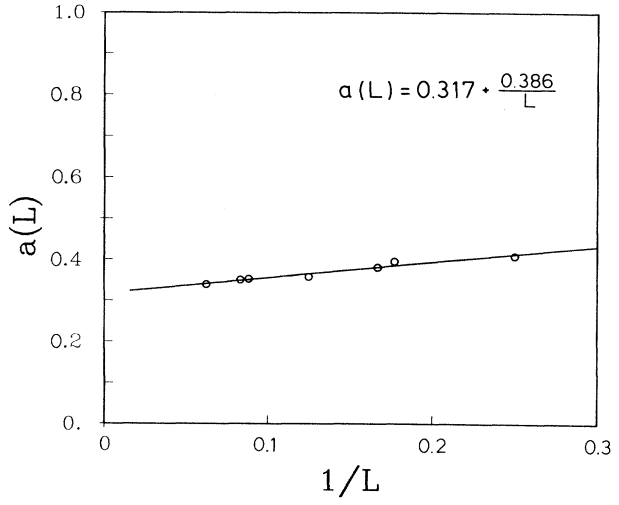

FIG. 16. Finite-size-scaling study of the spectral weight of the QP at $\mathbf{k} = (\pi/2, \pi/2)$ for $J = 0.4$. The numerical data for $a(\mathbf{k})$ calculated for systems of size $N = L \times L$ and L between 4 and 16 is consistent with a $1/L$ scaling. We see that the QP "survives" in the thermodynamic limit for this value of J.

V. RELATION TO EXPERIMENTS AND PREVIOUS WORK

The most direct experimental counterpart of our results pertains to angular-resolved ultraviolet photoemission spectroscopy. Recently this technique and also the inverse experiment (bremsstrahlung isochromat and x-ray absorption spectroscopy) have acquired such high resolution that the low-energy states (within 1 eV of the chemical potential), which have very small density of states, could be resolved for $Bi_2Sr_2CaCuO_8$.[34] The spectra in this range may be described as an almost structureless background with slight dispersive features superimposed (on the scale of J). Furthermore, a Fermi edge and the opening of the superconducting gap could also be observed.[35]

The weak dispersive experimental features are frequently taken as an indication for quasiparticle bands and as they seem to cross the Fermi level, it has been suggested that a Fermi liquid picture may apply. Such a conclusion seems somewhat premature in view of the data, and it has been strongly criticized.[36]

The calculation for a single hole suggests a natural explanation of the appearance of an almost structureless incoherent contribution. At finite hole concentration the incoherent part of the spectra is expected to become larger, as is in fact found in recent exact diagonalization studies.[37]

It appears tempting to assume that the results obtained for the single-hole case, in particular the hole pockets around $(\pi/2, \pi/2)$, characterize the low-energy charge excitations of HTSC's also at a finite doping concentration. Recently, Trugman[38] argued along these lines. In particular, he suggested that the hole pockets may provide a simple explanation for the change of sign of the Hall constant R_H at about 27% Sr doping in $La_{2-x}Sr_xCuO_4$.[39] As can be seen from the energy contours in Fig. (13) the hole pockets will be filled close to such a concentration and at higher doping the Fermi surface becomes "electronlike."

However, such a simple extrapolation of the single-hole result seems questionable as the spin correlations are strongly affected by doping. Diagonalization studies for the t-J model with finite doping[37] show that hole pockets are already absent at 10% doping for J values as large as $0.5t$. Both the momentum distribution $\langle n_k \rangle$ and the excitation spectra are compatible with a Fermi surface as given by noninteracting electrons in accordance with Luttinger's theorem. Similar conclusions for the 2D Hubbard model have been obtained recently by Monte Carlo simulations.[40]

A recent discussion of the spin-polaron concept with particular emphasis of the experimental situation in the context of high-T_c compounds has been given by Mott.[41]

VI. SUMMARY

We have studied the motion of a single hole in a 2D quantum antiferromagnet with a Green's function formalism. The approach presented here highlights in particular the close connection of the AF-spin polaron and the classical polaron problem.[42] The spin waves play the

role of the phonons in this case. We have pointed out that there are some differences. Particularly, there is no bare kinetic term for the holons in the t-J model. Nevertheless, the bound state describes a coherent motion on the scale of J. The coherent propagation is a result of the coupling H_t between the spinless fermion and spin waves. This is different from the usual notion in the polaron problem, where the mass of the particle becomes larger through the coupling.

The formulation in terms of spinless fermions automatically fulfills the constraint of no double occupancy. Nonetheless, an additional constraint is required to reduce the local Hilbert space spanned by a spinless fermion and a hard-core boson to the physical one.

However in the isotropic case ($\alpha = 1$), i.e., Heisenberg interaction, our results suggest that this constraint is of minor importance, at least for low hole doping.

The situation is different in the model with Ising interaction (t-J^z model). Only when the constraint is taken into account does the Born series become equivalent to the retraceable-path approximation. Processes not included in this series contain closed loops and are described as vertex corrections. These processes cause the delocalization of the hole in the Ising limit.

We have solved numerically the integral equation for the self-energy within the self-consistent Born approximation for a 2D square lattice in the isotropic case. Our results show that this approximation gives a good description for the spectral function, the spectral weight of the QP state and its dispersion. The bandwidth has a maximum at $J \simeq 0.8t$ and decays as $2t^2/J$ for large J, in agreement with Sachdev's variational result, which presumably includes all relevant physical processes. In particular, the direct comparison with exact diagonalization results for the spectral functions obtained with a 4×4 cluster shows a remarkable agreement and demonstrates that the self-consistent Born approximation is a valuable scheme for this class of problems. We stress that the equations work in the perturbative ($J \gg t$) and the strong-coupling regime ($J < t$). For the latter the self-consistent solution of the equations is crucial.

The study of the solution for large clusters reveals that convergence is already achieved for a cluster of size $N = 16 \times 16$ sites. The results for 8×8 and 16×16 clusters are almost indistinguishable on the scale plotted in Figs. 14 and 15. Hence they are expected to be representative for the results in the thermodynamic limit. Also very good agreement is found in comparing total energies with exact diagonalization results. Moreover, as is seen from finite-size-scaling analysis the spectral weight of the quasiparticle does not vanish in the thermodynamic limit for values of J/t typical for copper oxide superconductors.

Of course this does not answer an important question concerning the application of these results to high-T_c materials, namely, if at finite doping concentration quasiparticles close to the Fermi surface still exist or whether a Luttinger-liquid picture[36] or some other state,[43] characterized by a vanishing renormalization constant $Z = 0$ would emerge. The extension of this approach seems possible to finite hole concentration and for finite temperatures. Also the choice of certain spin-liquid–type ground states, without long-range AF order, may be of considerable interest.

When completing this manuscript we received a preprint from Marsiglio, Ruckenstein, Schmitt-Rink, and Varma who also report the observation of the surprising quality of the Born approximation.[46]

ACKNOWLEDGMENTS

We would like to thank P. Fulde, K. J. von Szczepanski, W. Stephan, J. Zaanen, and M. Ziegler for many helpful discussions, as well as A. L. Kuzemsky and A. M. Oleś for careful reading of the manuscript. Furthermore we would like to thank F. Marsiglio for sending their manuscript prior to publication. One of us (G.M.) acknowledges partial support from a Brazilian agency (Coordenaçåo de Aperfeiçoamento de Pessoal do Ensino Superior) during part of his stay at the Max-Planck-Institut.

APPENDIX: RELATION BETWEEN ELECTRON AND HOLON GREEN'S FUNCTION

The electron Green's function Eq. (2) may be written as

$$G_\sigma(k,\omega) = \left\langle \psi_0 \left| c^\dagger_{k\sigma} \frac{1}{\omega - H + E_0} c_{k\sigma} \right| \psi_0 \right\rangle. \tag{A1}$$

Using Eq. (7) the annihilation operator $c_{k\sigma}$ ($\sigma = \uparrow$) may be decomposed into two separate contributions coming from the two sublattices A and B. Taking care of the sublattice rotation Eq. (3) one arrives at

$$c_{k\uparrow} = \frac{1}{\sqrt{N}} \left(\sum_{i \in A} e^{-ikx_i} h^\dagger_i a_i a^\dagger_i + \sum_{j \in B} e^{-ikx_j} h^\dagger_j a_j \right). \tag{A2}$$

Here the additional factor $a_i a^\dagger_i$ on the right-hand side of Eq. (A2) enforces the constraint [C1], that a hole should not be created at a site when a spin deviation is present in $|\psi_0\rangle$. Given a ground state $|\psi_0\rangle$ with quantum fluctuations, Eq. (18), the operators $(a_i a^\dagger_i)$ and a_j determine the probability to find an up spin on the A and B sublattice, respectively.

Considering this effect on the average we may write

$$c_{k\uparrow} = \frac{1}{\sqrt{N}} \left(\sqrt{1-n_0} \sum_{i \in A} e^{-ikx_i} h^\dagger_i + \sqrt{n_0} \sum_{j \in B} e^{-ikx_j} h^\dagger_j \right)$$

$$= \frac{1}{\sqrt{2}} (\sqrt{1-n_0}\, h^\dagger_{k,A} + \sqrt{n_0}\, h^\dagger_{k,B}). \tag{A3}$$

where $(1 - n_0)$ and n_0 define the probabilities to find an $\uparrow$ spin on the A or B sublattice, respectively. The spin

deviations are given by $n_0 = \langle a_i^\dagger a_i \rangle = \frac{1}{2} - \langle S_i^z \rangle \approx 0.2$ in 2D.

The Green's function may then be written as

$$G_\uparrow(k,\omega) = \tfrac{1}{2}\{ (1-n_0)G^h_{AA}(k,\omega) + n_0 G^h_{BB}(k,\omega) + \sqrt{1-n_0}\sqrt{n_0}[G^h_{AB}(k,\omega) + G^h_{BA}(k,\omega)]\}, \quad \text{(A4)}$$

where the prefactors give the statistical weights to find an $\uparrow$ spin on the A or B sublattice, respectively.

The implicit assumption here is that the orientation of the spin removed when creating the hole is of no further relevance. What counts is only the propagation of the "spinless" hole and its interaction with the remaining spins due to its motion.

Defining the Green's function for holons (spinless fermions) as

$$G^h(k,\omega) = \left\langle 0 \left| h_k \frac{1}{\omega - H + E_0} h_k^\dagger \right| 0 \right\rangle, \quad \text{(A5)}$$

with $h_k^\dagger = (1/\sqrt{2})(h^\dagger_{k,A} + h^\dagger_{k,B})$, and $|0\rangle$ being the vacuum for both holes and spin excitations. Since the intersublattice Green's functions G_{AB}, G_{BA} vanish in the problem treated above, and as $G^h_{AA} = G^h_{BB}$ it is evident from (A4) that

$$G_\uparrow(k,\omega) \cong G^h(k,\omega). \quad \text{(A6)}$$

This consideration also suggests that this close correspondence will disappear for a spin background without staggered long-range order, i.e., where the contributions from the intersublattice Green's functions become substantial. An example is the t-J model in 1D, where the spectral function is given as a continuum with a momentum dependence resulting from such processes.[11,44,45]

[1] J. G. Bednorz and K. A. Müller, Z. Phys. B **64**, 189 (1986).
[2] Y. Tokura, H. Takagi, and S. Uchida, Nature **337**, 345 (1989).
[3] G. Shirane, Y. Endoh, R. J. Birgeneau, M. A. Kastner, Y. Hidaka, M. Oda, M. Suzuki, and T. Murakami, Phys. Rev. Lett. **59**, 1613 (1987).
[4] P. W. Anderson, Science **235**, 1196 (1987); in *Frontiers and Borderlines in Many-Particle Physics*, Proceedings of the International School of Physics "Enrico Fermi," Course 104, Varenna, 1987, edited by R. A. Broglia and J. R. Schrieffer (North-Holland, Amsterdam, 1989).
[5] L. N. Bulaevskii, E. Nagaev, and D. L. Khomskii, Sov. Phys. JETP **27**, 836 (1968); J. E. Hirsch, Phys. Rev. Lett. **54**, 1317 (1985); C. Gros, R. Joynt, and T. M. Rice, Phys. Rev. B **36**, 381 (1987).
[6] V. J. Emery, Phys. Rev. Lett. **58**, 2794 (1987).
[7] F. C. Zhang and T. M. Rice, Phys. Rev. B **37**, 3759 (1988).
[8] H. Eskes and G. A. Sawatzki, Phys. Rev. Lett. **61**, 1415 (1988).
[9] P. Horsch, W. Stephan, K. J. von Szczepanski, M. Ziegler, and W. von der Linden, Physica C **162**, 783 (1989); P. Horsch, Helv. Phys. Acta **63**, 346 (1990).
[10] S. A. Trugman, Phys. Rev. B **41**, 892 (1990).
[11] K. J. von Szczepanski, P. Horsch, W. Stephan, and M. Ziegler, Phys. Rev. B **41**, 2017 (1990).
[12] E. Dagotto, R. Joynt, A. Moreo, S. Bacci, and E. Gagliano, Phys. Rev. B **41**, 9049 (1990).
[13] I. Sega and P. Prelovšek, Phys. Rev. B **42**, 892 (1990); J. Inoue and S. Maekawa, J. Phys. Soc. Jpn. **59**, 2110 (1989).
[14] S. Schmitt-Rink, C. M. Varma, and A. E. Ruckenstein, Phys. Rev. Lett. **60**, 2793 (1988).
[15] C. L. Kane, P. A. Lee, and N. Read, Phys. Rev. **39**, 6880 (1989).
[16] Z. B. Su, Y. M. Li, W. Y. Lai, and L. Yu, Phys. Rev. Lett. **63**, 1318 (1989).
[17] A. Ramšak and P. Prelovšek, Phys. Rev. B **42**, 10 415 (1990); N. Furukawa and M. Imada, J. Phys. Soc. Jpn. **59**, 1771 (1990).
[18] B. S. Shastry and D. C. Mattis, Phys. Rev. B **24**, 5340 (1981).
[19] G. Martinez and P. Horsch, Int. J. Mod. Phys. B **5**, 207 (1991).
[20] B. I. Shraiman and E. D. Siggia, Phys. Rev. Lett. **60**, 740 (1988); **61**, 467 (1988).
[21] W. F. Brinkman and T. M. Rice, Phys. Rev. B **2**, 1324 (1970).
[22] E. L. Nagaev, Sov. Phys. JETP **27**, 122 (1968).
[23] P. W. Anderson, Phys. Rev. **86**, 694 (1952).
[24] R. Kubo, Phys. Rev. **87**, 568 (1952).
[25] P. Horsch and W. von der Linden, Z. Phys. B **72**, 181 (1988).
[26] D. A. Huse and V. Elser, Phys. Rev. Lett. **60**, 2531 (1988); N. Trivedi and D. Ceperley, Phys. Rev. B **40**, 2737 (1989); M. Gross, E. Sanchez-Velasco, and E. D. Siggia, *ibid.* **40**, 11 328 (1989); Z. Liu and E. Manousakis, *ibid.* **40**, 11 437 (1989).
[27] D. C. Mattis, in *The Theory of Magnetism I*, edited by P. Fulde, Springer Series in Solid-State Physics, Vol. 17 (Springer, Berlin, 1981).
[28] G. D. Mahan, *Many-Particle Physics*, 2nd ed. (Plenum, New York, 1990).
[29] D. Pines, in *Polarons and Excitons*, edited by C. G. Kuper and G. D. Whitfield (Oliver and Boyd, Edinburgh, 1962); J. Appel, in *Solid State Physics*, Vol. 21, edited by F. Seitz, D. Turnbull, and H. Ehrenreich (Academic, New York, 1968).
[30] L. N. Bulaevskii, E. L. Nagaev, and D. L. Khomskii, Sov. Phys. JETP. **27**, 836 (1968).
[31] S. A. Trugman, Phys. Rev. **37**, 1597 (1988).
[32] R. Eder and K. W. Becker, Z. Phys. B **78**, 219 (1990).
[33] S. Sachdev, Phys. Rev. B **39**, 12 232 (1989).
[34] T. Takahashi, H. Matsuyama, H. Katayama-Yoshida, Y. Okabe, S. Hosoya, K. Seki, H. Fujimoto, M. Sato, and H. Inokuchi, Nature **334**, 691 (1988); Phys. Rev. B **39**, 236 (1989); G. Mante, R. Claessen, T. Buslaps, S. Harm, R. Manzke, M. Shibowski, and J. Fink, Z Phys. B **80**, 181 (1990); C. G. Olson, R. Liu, D. W. Lynch, R. S. List, A.

J. Arko, B. W. Veal, Y. C. Chang, P. Z. Jiang, and A. P. Paulikas, Phys. Rev. B **42**, 381 (1990).
[35] J. M. Imer, F. Patthey, B. Dardel. W. D. Schneider, Y. Baer, Y. Petroff, and A. Zettl, Phys. Rev. Lett. **62**, 336 (1989).
[36] P. W. Anderson, Phys. Rev. Lett. **64**, 1839 (1990); Int. J. Mod. Phys. B **4**, 181 (1990).
[37] W. Stephan and P. Horsch, Phys. Rev. Lett. **66**, 2258 (1991).
[38] S. A. Trugman, Phys. Rev. Lett. **65**, 500 (1990).
[39] S. Uchida, H. Takagi, Y. Tokura, N. Koshihara, and T. Arima, in *Strong Correlation and Superconductivity*, edited by H. Fukuyama, S. Maekawa, and A. P. Malozemoff, Springer Series in Solid-State Sciences, Vol. 89 (Springer, Berlin, 1989).
[40] A. Moreo, D. J. Scalapino, R. L. Sugar, S. R. White, and N. E. Bickers, Phys. Rev. B **41**, 2313 (1990).
[41] N. F. Mott, Adv. Phys. **39**, 55 (1990).
[42] J. T. Devreese, in *Polarons and Excitons in Polar Semiconductors*, Vol. 108 of *NATO Advanced Study Institute, Series B: Physics*, edited by J. T. Devreese and F. Peeters (Plenum, New York, 1984).
[43] C. M. Varma, Int. J. Mod. Phys. B **3**, 2083 (1989).
[44] W. Brenig and K. W. Becker, Z. Phys. B **76**, 473 (1989).
[45] M. Ziegler and P. Horsch, in *Proceedings of the NATO Advanced Research Workshop on Dynamics of Magnetic Fluctuations in High Temperature Superconductors*, edited by G. Reiter, P. Horsch, and G. Psaltakis (Plenum, New York, 1991).
[46] F. Marsiglio, A.E. Ruckenstein, S. Schmitt-Rink, and C.M. Varma (unpublished).